Langmuir

Article

pubs.acs.org/Langmuir

Nanoparticle–Protein Interactions: A Thermodynamic and Kinetic Study of the Adsorption of Bovine Serum Albumin to Gold Nanoparticle Surfaces

Stefano P. Boulos,[†] Tyler A. Davis,[‡] Jie An Yang,[†] Samuel E. Lohse,[†] Alaaldin M. Alkilany,[§] Lisa A. Holland,[‡] and Catherine J. Murphy*,[†]

[†]Department of Chemistry, University of Illinois at Urbana–Champaign, 600 South Mathews Avenue, Urbana, Illinois 61801, United States

[‡]C. Eugene Bennett Department of Chemistry, West Virginia University, 217 Clark Hall, Prospect Street, Morgantown, West Virginia 26506, United States

[§]Department of Pharmaceutics & Pharmaceutical Technology, Faculty of Pharmacy, The University of Jordan, Amman 11942, Jordan

Supporting Information

ABSTRACT: Investigating the adsorption process of proteins on nanoparticle surfaces is essential to understand how to control the biological interactions of functionalized nanoparticles. In this work, a library of spherical and rod-shaped gold nanoparticles (GNPs) was used to evaluate the process of protein adsorption to their surfaces. The binding of a model protein (bovine serum albumin, BSA) to GNPs as a function of particle shape, size, and surface charge was investigated. Two independent comparative analytical methods were used to evaluate the adsorption process: steady-state fluorescence quenching titration and affinity capillary electrophoresis (ACE). Although under favorable electrostatic conditions kinetic analysis showed a faster adsorption of BSA to the surface of cationic GNPs, equilibrium binding constant determinations indicated that BSA has a comparable binding affinity to all of the GNPs tested, regardless of surface charge. BSA was even found to adsorb strongly to GNPs with a pegylated/neutral surface. However, these fluorescence titrations suffer from significant interference from the strong light absorption of the GNPs. The BSA–GNP equilibrium binding constants, as determined by the ACE method, were 10^5 times lower than values determined using spectroscopic titrations. While both analytical methods could be suitable to determine the binding constants for protein adsorption to NP surfaces, both methods have limitations that complicate the determination of protein–GNP binding constants. The optical properties of GNPs interfere with K_a determinations by static fluorescence quenching analysis. ACE, in contrast, suffers from material compatibility issues, as positively charged GNPs adhere to the walls of the capillary during analysis. Researchers seeking to determine equilibrium binding constants for protein–GNP interactions should therefore utilize as many orthogonal techniques as possible to study a protein–GNP system.

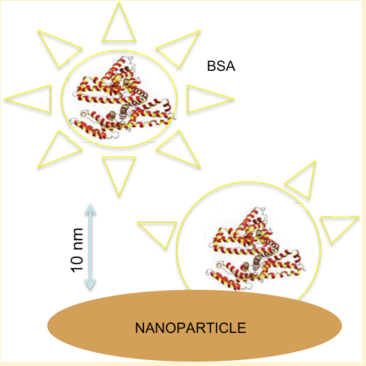

INTRODUCTION

In the past decade, gold nanoparticles (GNPs) have been the subject of much scientific interest due to their size-tunable optical properties.[1] Chemists have made important progress in precisely controlling GNP sizes and shapes, as well as their surface chemistries using a multitude of syntheses.[2] Such progress has opened a variety of biological applications for GNPs, which include, but are not limited to, chemical sensing, imaging, and drug delivery.[1−5] Controlling GNP interactions in biological systems requires more than just physiochemical property control during synthesis. It also requires a fundamental understanding of GNP–biological interactions, including the interactions of GNPs with simple biomacromolecules.

It is now widely accepted that a protein corona rapidly forms on GNP surfaces when introduced into a biological medium.[6] The adsorption of proteins to the surface of the GNP can significantly change the surface charge of the GNPs, which has important consequences for NP fate and transport in biological systems. Therefore, the composition of the protein corona largely defines the biological identity of the nanoparticle. In addition, because of their extremely large surface area to volume ratios, a significant number of proteins can be adsorbed and "trapped" on GNP surfaces when they are introduced into biological entities.[6−11] Coupled with GNPs' small size and accessibility to almost every organ in vivo,[12,13] understanding and controlling the NP–biological interaction is crucial to fully realize GNPs' potential in biomedicine.

The protein corona–NP complex is a dynamic system. Therefore, parameters such as binding affinities and rates of

Received: July 31, 2013
Revised: November 9, 2013

   dx.doi.org/10.1021/la402920f | Langmuir XXXX, XXX, XXX–XXX

protein adsorption/desorption are important to understand how nanoparticles are "seen" by cells as they travel in biological systems.[14] Gathering thermodynamic and kinetic data on the interaction of proteins with nanoparticles is necessary to develop a framework that will allow for the prediction of how cellular systems will respond to the presence of nanoparticles based on their size, curvature, and charge.

For GNPs, a variety of different analytical techniques have been used to investigate protein−GNP interactions. Spectroscopic techniques are used to determine binding affinity, the ratio of protein to GNP, and the mechanism of the adsorption of proteins to nanomaterial surfaces. Most published work employs optical techniques such as UV−vis spectrophotometry,[15,16] fluorescence,[17−20] circular dichroism,[15,21,22] and dynamic light scattering[20,23,24] to probe the interaction of proteins with nanomaterials. Those methods allow a direct measurement of the adsorption process without the need to separate free versus bound proteins. However, these methods suffer from gold nanoparticle spectral interference due to the high extinction coefficient of these gold nanomaterials, especially gold nanorods (GNRs).[25,26] Previous studies of protein binding to GNPs have yielded equilibrium binding constants with a wide range of values, spanning 8 orders of magnitude, depending on the exact system and buffer conditions (vide infra). Vastly different binding constants have been reported even for similar protein−GNP systems investigated using the same analytical techniques. At this time, it is not clear that a single analytical approach can be utilized for accurate binding constant determinations, as each technique has strengths and weaknesses. Therefore, it is essential to determine protein−NP binding constants by multiple techniques whenever possible.

In this work, we investigate the thermodynamics and kinetics of a model protein, bovine serum albumin (BSA), adsorbing to the surface of both spherical and rod-shaped GNPs using two independent and comparative analytical methods. GNPs were selected as a model engineered NP due to their interesting optical properties. Furthermore, their size, shape, and charge can be controlled using simple chemistries.[27] Similarly, BSA is an important model protein, because it is an abundant plasma protein in mammals and highly stable. BSA contains tryptophan residues, which makes it absorb and fluoresce light at characteristic wavelengths. These characteristics are useful for studying protein binding using spectroscopic measurements.[28]

We prepared a library of functionalized GNPs including gold nanospheres (20 nm) and gold nanorods (GNRs) with two different aspect ratios (3.5 and 18) and functionalized them to give GNPs with three different surface chemistries. We then used absorbance spectroscopy to determine rate constants for BSA binding to GNRs with different surface charges. Subsequently, we used two analytical techniques to determine the equilibrium binding constants of BSA to our GNP library. The first analytical method used to study BSA−GNP interactions was steady-state fluorescence spectroscopy, which takes advantage of the fluorescence quenching capability of the GNPs to quantify protein adsorption. Salt-dependent titration experiments allowed us to extract the degree to which electrostatics plays a role in the nanoparticle−protein binding event. A second analytical method, affinity capillary electrophoresis (ACE), was also used to quantify BSA−GNP binding. This method relies on the detection of shift in mobility of the GNPs in the presence of BSA as they travel through a capillary. It is an attractive technique that can be used to distinguish free nanoparticles from protein bound nanoparticles without the use of potentially harsh sample treatment steps such as centrifugation. After determining the equilibrium binding constants for BSA adsorption to each of the GNPs studied, we compare the relative advantages and disadvantages of using fluorescence spectroscopy and ACE to monitor the protein adsorption process.

EXPERIMENTAL SECTION

Materials. Chloroauric acid ($HAuCl_4{\cdot}3H_2O$, 99.9%), sodium borohydride ($NaBH_4$, 99%), silver nitrate ($AgNO_3$, 99+%), cetyltrimethylammonium bromide (CTAB, 99%, Sigma Ultra), ascorbic acid (99+%), poly(acrylic acid, sodium salt), ∼15 000 g/mol, 35 wt % in water, and poly(allylamine hydrochloride), ∼15 000 g/mol, were obtained from Sigma-Aldrich and used as received. Thiolated poly(ethylene glycol), 5000 g/mol, was purchased from Nanocs. Bovine serum albumin (BSA) used for the CE experiments was RIA grade, lipid free (E588-25G, lot no. 0641C081, Amresco). For CE, the protein was weighed out each day it was to be used to make a 1000 μM stock solution, which was then diluted to concentrations required for the experiments in 5 mM MOPS. For other experiments, BSA was purchased from Sigma Life Sciences, and the protein from one batch was used in all experiments. 3-(*N*-Morpholino)-propanesulfonic acid (MOPS) was purchased from Alfa Aesar. All GNP solutions were prepared with purified 18 MΩ water. Glassware was cleaned with aqua regia and rinsed thoroughly with nanopure deionized water.

Instrumentation. Absorption spectra were taken on a Cary 500 scan UV−vis−NIR spectrophotometer. Transmission electron microscopy (TEM) data were obtained with a Jeol 2100 Cryo electron microscope operating at 200 kV. TEM grids were prepared by drop casting 10 μL of purified gold nanoparticle solution on the TEM grids and drying them in air. Zeta potential measurements were performed on a Brookhaven Zeta PALS instrument. Fluorescence measurements were performed on a Jobin Yvon Horiba Fluoromax-3 spectrophotometer. A Hewlett-Packard 8453 spectrophotometer was used to collect kinetic data of the adsorption process at fast rates (10 spectra/s). Capillary electrophoresis separation was performed on a P/ACE MDQ system (Beckman Coulter, Fullerton, CA) equipped with a photodiode array detector.

Synthesis of CTAB-Capped Gold Nanorods (Aspect Ratio = 3.5 and 18). Gold nanorods were prepared using a simple wet chemical method in the presence of the surface capping agent cetyltrimethylammonium bromide as previously described.[2,29−31] A solution of 2.5×10^{-4} M $HAuCl_4$ was prepared in 0.1 M aqueous CTAB in a 50 mL centrifuge tube. $NaBH_4$ (600 μL, of a 10 mM stock solution) was added to the gold/CTAB solution (10 mL) with vigorous stirring for 10 min with the help of a stir bar. The resulting seed particles (∼3 nm diameter) were used for the synthesis of both short and long gold nanorods. For the short gold nanorods (aspect ratio 3.5), the following were added, in order, to a conical flask: CTAB solution (95 mL of a 0.1 M stock solution), silver nitrate solution (1 mL of a 10 mM stock solution), and $HAuCl_4$ (5 mL of a 10 mM stock solution). An aqueous solution of ascorbic acid (0.55 mL of a 0.1 M stock solution) was then added with gentle mixing. Finally, the gold seed solution (0.12 mL) was added and mixed. The solution was left undisturbed overnight. The colored gold nanorod solution was purified by centrifugation (2×) to remove excess CTAB. The method yielded gold nanorods of length 54.0 ± 2.1 nm and width 15.9 ± 1.1 nm.

For the long gold nanorods (AR 18), a three-step seeding procedure was used.[31] First, the following were added to two 15 mL centrifuge tubes: $HAuCl_4$ (250 μL of 0.01 M stock solution) and aqueous CTAB (9 mL of 0.1 M CTAB stock solution) to each centrifuge tube. To these mixtures, ascorbic acid was added (50 μL of 0.1 M stock solution) to each tube and mixed. In parallel, the following was added to a 200 mL conical flask: $HAuCl_4$ (2.5 mL of 0.01 M stock solution) and aqueous CTAB (90 mL of 0.1 M CTAB stock solution). To this flask, 0.5 mL of ascorbic acid (0.1 M stock solution) was added. To the

dx.doi.org/10.1021/la402920f | *Langmuir* XXXX, XXX, XXX−XXX

first 15 mL centrifuge tube was added 1 mL of seed; after 15 s, 1 mL of this solution was added to the second centrifuge tube. After 30 s, the entire content of this solution was added to the 200 mL flask, and the solution was gently mixed and stored for about 14 h. After 14 h, the content of the flask was discarded leaving the long gold nanorods deposited at the bottom. These rods were suspended by washing the inside of the flask with purified water. Excess CTAB was removed through centrifugation. The method yielded gold nanorods of length 342 ± 65 nm and width 21.1 ± 2.6 nm.

Synthesis of 20 nm CTAB-Capped Nanospheres. Twenty nanometer CTAB-capped spheres were prepared using the method described previously.[32] Citrate-capped gold seeds were prepared by reducing a solution of 0.5 mL of $HAuCl_4$ (0.01 M), 19 mL of deionized H_2O, and 0.5 mL of trisodium citrate (0.01 M) with 0.6 mL of 0.1 M sodium borohydride. A growth solution was prepared by mixing 6 g of solid CTAB (0.08 M final concentration) with $HAuCl_4$ (2.5×10^{-4} M final concentration) in purified water. The growth solution was heated until it turned clear orange. Two sets of 50 mL conical flasks were labeled A and B. In flask A, 9 mL of growth solution and 0.05 mL of 0.1 M ascorbic acid were mixed, and 1 mL of the gold seed was added while stirring. The solution was stirred for 10 min giving a final deep red color. Particles prepared this way are about 8 nm in diameter and were used as seed to prepare 20 nm spheres. In flask B, 9 mL of growth solution was mixed with 0.05 mL of ascorbic acid, and 1 mL from set A was added while stirring. The solution was stirred for 10 min, and the final color of the solution was reddish brown. Excess CTAB was removed through centrifugation at 8000 rpm for 30 min followed by redispersion in deionized water (twice). This method yielded gold nanospheres of diameter 21.5 ± 1.1 nm.

Polyelectrolyte Coating of Gold Nanoparticles. GNPs coated with different layers of polyelectrolytes were prepared using a layer-by-layer adsorption technique.[33] Sodium poly(acrylic acid) (PAA) and poly (allylamine hydrochloride) (PAH), each with a molecular weight of approximately 15 000 g/mol, were used. A 200 μL volume of polyelectrolyte solution (10 mg/mL prepared in 10 mM NaCl solution) and 100 μL NaCl solution (10 mM) were added simultaneously to every 1 mL of purified CTAB-capped GNPs solution of different shape and size. The resulting solution was mixed gently and incubated overnight to allow for complete polymer coating. To remove the excess polyelectrolyte in solution, GNPs were centrifuged at 7000 rpm for 30 min and redispersed in water. GNPs were further dialyzed against water for 24 h to ensure removal of excess reagents using 20K MWCO dialysis cassettes.

Preparation of Thiolated Polyethylene Glycol (PEG)-Capped Gold Nanoparticles. Synthesized gold nanoparticles of different shape and size were capped with a thiolated polyethylene glycol (mPEG-SH) through displacement of CTAB at the surface of the gold nanoparticles.[34] A 100 mL aqueous solution of as-prepared gold nanoparticles was concentrated to 0.5 mL via centrifugation. Next, 2 mL of mPEG-SH (5000 g/mol) at concentration 20 mg/mL was prepared and sonicated for 15 min. This solution was added dropwise under vigorous stirring to the CTAB-capped gold particle solution. The mixture was allowed to react for 12 h. The PEG-capped gold nanoparticles were purified by centrifugation at 7000 rpm for 30 min and redispersed in water. GNPs were further dialyzed for 24 h to ensure removal of excess reagents using 20K MWCO dialysis cassettes.

Steady-State Fluorescence Quenching Measurements. For the fluorescence quenching measurements, the emission of BSA was measured at a constant concentration (0.66 μM) in the presence of an increasing concentration of gold nanoparticles (0–3 nM in particles). 3-Morpholinopropane-1-sulfonic acid buffer (MOPS, 5 mM, pH 7) and nanopure water were used as solvents. The nanoparticle–protein solutions were incubated overnight at 4 °C to ensure equilibrium in Teflon vials. Before the fluorescence of BSA was measured, solutions were allowed to stand at room temperature for 30 min. The samples were then transferred to a quartz cuvette, and their fluorescence spectra were acquired in the range of 300–460 nm when excited at 280 nm. Because the fluorescence of BSA protein adsorbed to the surface of the GNPs is quenched, the observed fluorescence is due to the free BSA in the solution. The area under each fluorescence curve was integrated and used to measure the free BSA concentration using a standard calibration curve.

Capillary Electrophoresis Measurements. A bare fused silica capillary with a 50 μm internal diameter and 360 μm outer diameter (Polymicro Technologies, Phoenix, AZ) with an effective length of 20.0 cm and a total length of 30.2 cm was used for all separations. Capillaries were subject to the following flushing sequence daily: 1 M NaOH for 30 min at 69 kPa (10 psi), deionized water for 15 min at 69 kPa (10 psi), 15 min with methanol at 69 kPa (10 psi), deionized water for 15 min at 69 kPa (10 psi). Prior to each electrophoretic separation, the separation capillary was flushed as follows: 1 M NaOH for 1 min at 69 kPa (10 psi), methanol for 1 min at 69 kPa (10 psi), deionized water for 2 min at 69 kPa (10 psi), and 5 mM MOPS for 3 min at 69 kPa (10 psi). BSA was included in the running buffer at different concentrations (0–200 μM). To prevent aggregation of the nanoparticles upon addition of the dimethylformamide neutral marker to the nanoparticle stock, serial injection was used. The dimethylformamide diluted in 5 mM MOPS was introduced first with a pressure of 3 kPa (0.5 psi) for 5 s. The gold nanoparticles were then injected at ~7 nM using a pressure of 7 kPa (1 psi) for 4 s. When smaller injection volumes were used, the nanoparticles could not be detected. Separations were accomplished using normal polarity with an applied voltage of 6 kV (E = 200 V/cm) and 12 kV (E = 400 V/cm) for neutral and negative nanoparticles, respectively. Data collection and analysis were performed using 32 Karat Software version 5.0 (Beckman Coulter). Binding curves were analyzed using Graphpad Prism Version 4.00 (Graphpad Software, San Diego, CA) curve-fitting software for nonlinear regression.

RESULTS AND DISCUSSION

Gold Nanoparticles Synthesis and Functionalization. GNPs of different size and shape were prepared according to our standard procedures.[2] Three types of GNPs were used: 20 nm gold nanospheres, gold nanorods with aspect ratio 3.5, and gold nanorods with aspect ratio 18 (Figure 1). GNP concentrations were determined on the basis of the extinction coefficient at transverse/longitudinal plasmon peak maxima, as previously reported. GNPs surface charge was varied using a layer-by-layer polyelectrolyte deposition method that was

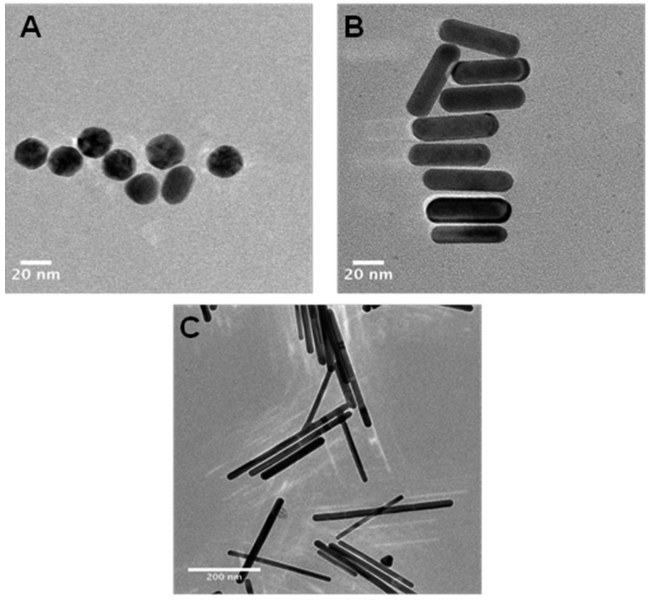

Figure 1. Transmission electron micrographs of (A) gold nanospheres of diameter ~20 nm; (B) short gold nanorods of aspect ratio 3.5; and (C) long gold nanorods of aspect ratio 18. Scale bars for (A) and (B) are 20 nm; the scale bar for (C) is 200 nm.

dx.doi.org/10.1021/la402920f | Langmuir XXXX, XXX, XXX–XXX

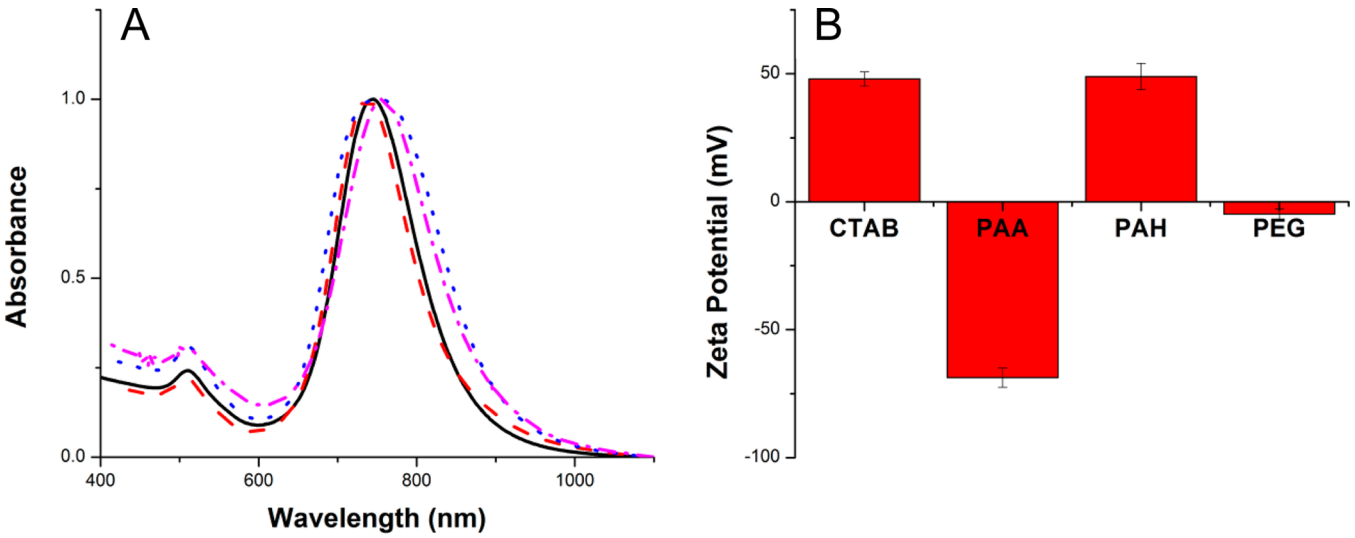

Figure 2. (A) UV−vis absorbance of aspect ratio 3.5 GNRs capped with a CTAB bilayer (−), after being wrapped with the negatively charged polyelectrolyte PAA via electrostatic interaction (− − −), with a second layer of the positively charged polyelectrolyte PAH (− · − · −), and after displacing the CTAB using a thiolated PEG to form PEG-capped GNRs (···). (B) ζ-Potential measurements show changes in surface charge as gold nanoparticles are functionalized with different polymers.

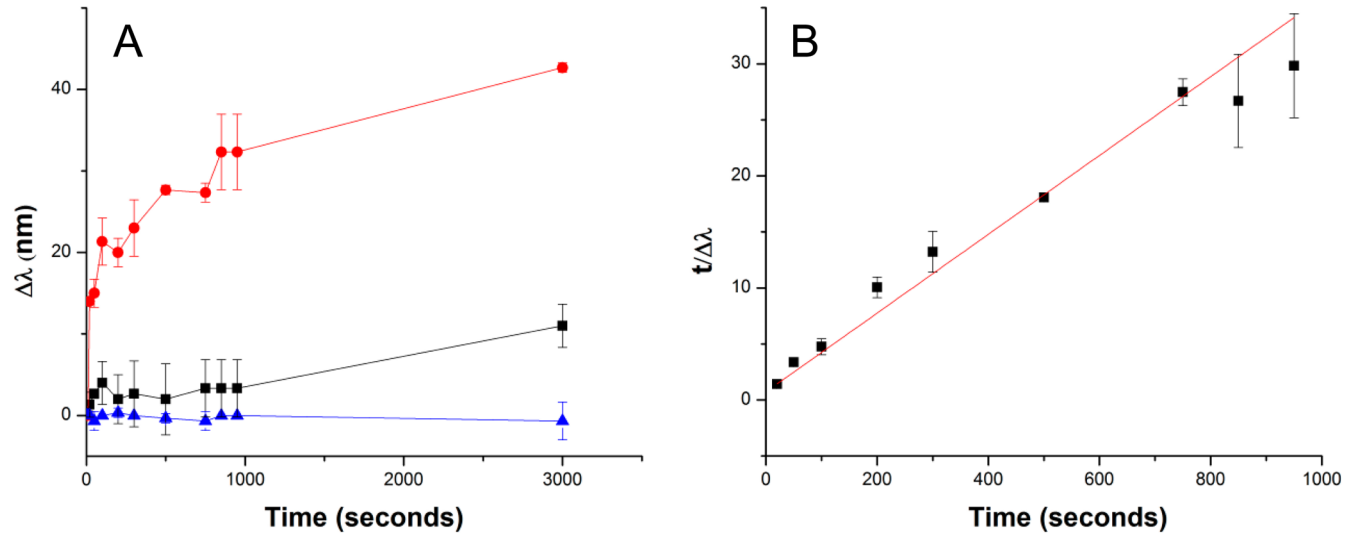

Figure 3. Longitudinal plasmon resonance peak shift of GNRs over a short time scale (0−1000 s) as BSA is introduced to GNR solutions (AR 3.5). (A) PAA−GNRs (black dots) show a small red shift of ∼5 nm after ∼100 s; PAH−GNRs (red dots) show a red shift of ∼20 nm immediately after BSA addition; and PEG−GNRs (blue dots) show no significant shift. (B) A linear pseudo-second-order kinetic curve for BSA adsorbing to PAH−GNRs.

previous developed.[33] As-prepared, GNPs originally had a coating of CTAB (cationic) on the surface. An anionic polyelectrolyte (sodium polyacrylate, PAA, MW = 15 000 g/mol) was used to overcoat these GNPs, conferring a negative surface charge on GNPs. These anionic GNPs were subsequently coated with additional cationic polyelectrolyte (polyallylamine hydrochloride, PAH, MW = 15 000 g/mol), thus producing GNPs with a positively charged surface. PEG-coated GNPs were prepared by ligand exchange with a thiolated-PEG-methoxy polymer (MW = 5000 g/mol).

To prevent possible protein binding by free ligands in solution, care was taken to ensure the removal of free ligands from the GNP solutions. Initial CTAB−GNP solutions were purified twice by centrifugation and washing. In addition, after each surface functionalization step, GNPs were again purified via centrifugation and washing followed by dialysis in 1 L Millipore water for at least 24 h, with two water replacement steps during that period of time.

Upon surface coating and purification, the plasmon peak maximum in the UV−vis spectra of all GNP solutions was shifted, signifying a change in the dielectric constant around the GNP (i.e., a change in surface ligands (Figure 2a, Supporting Information Figure S1)). Similarly, ζ-potential measurements also showed the change in surface charges, reflecting the corresponding change in surface functionalization of the GNPs (Figure 2b).

Kinetic Study of the Adsorption of BSA to the Surface of Functionalized GNRs. Prior to investigating the equilibrium binding behavior of BSA adsorbed to the GNPs, we undertook a brief kinetic investigation to determine the approximate time required for the BSA to saturate the GNP surface. For these kinetic experiments, we focused on the short

dx.doi.org/10.1021/la402920f | *Langmuir* XXXX, XXX, XXX−XXX

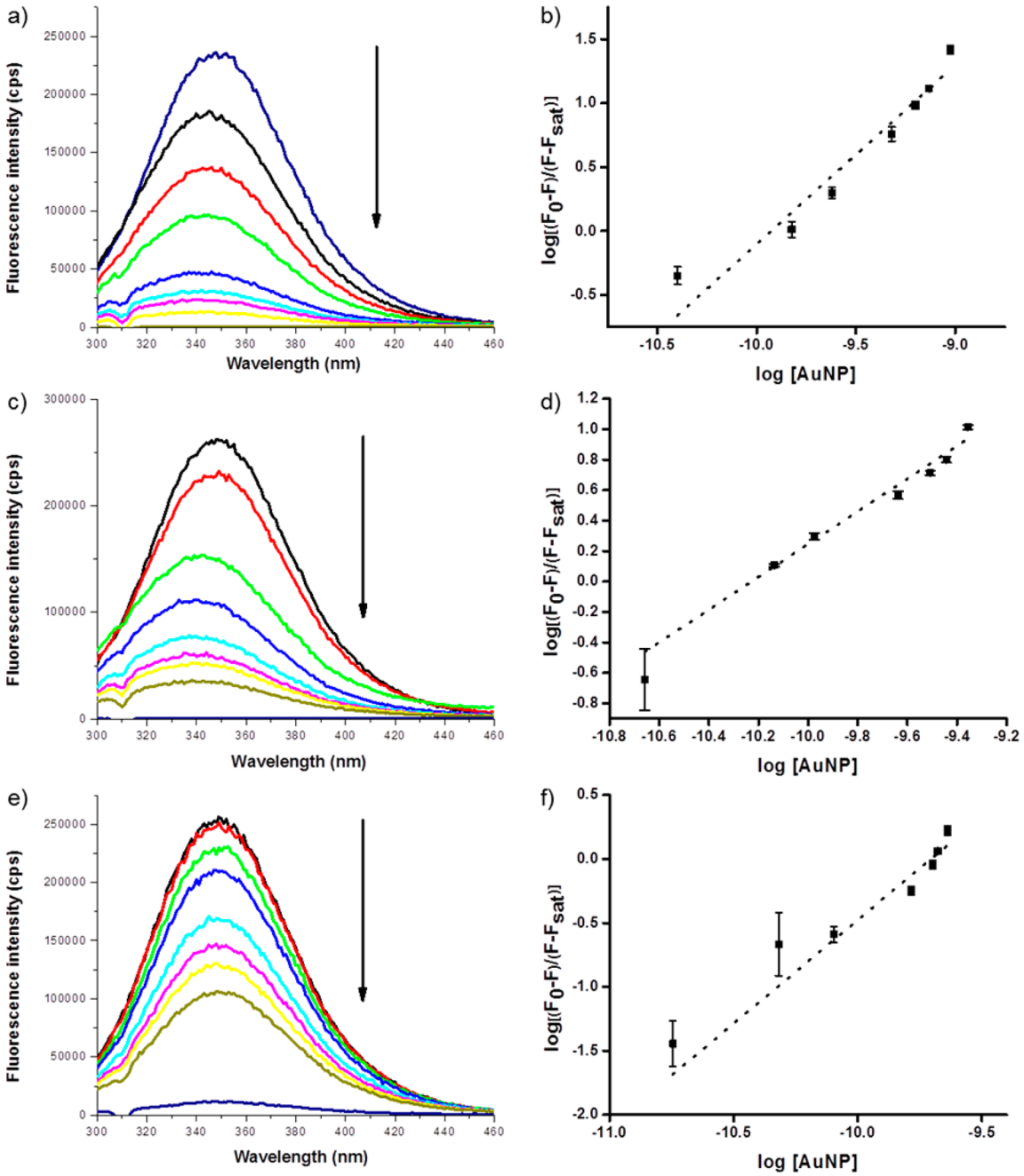

Figure 4. Fluorescence spectra of BSA at 0.66 μM with increasing concentration (0−3 nM) of differently charged GNRs (AR 3.5) showing the decrease in protein fluorescence with increasing concentration of GNRs: (a) PAA−GNRs; (c) PAH−GNRs; and (e) PEG−GNRs. Figure 4. Double logarithmic plot, derived from fluorescence data, depicting the binding curves resulting from the adsorption of BSA to GNRs for different surface chemistries: (b) PAA−GNRs; (d) PAH−GNRs; and (f) PEG−GNRs. Best-fit lines are shown with the data points.

GNRs (AR 3.5). To investigate the rate of adsorption of BSA on different gold nanorod surfaces, we took advantage of the sensitivity of the longitudinal plasmon band of the GNR to the local dielectric environment, and measured the rate of BSA binding as a function of the change in the plasmon λ_{max} over time. A photodiode array spectrophotometer was used to monitor the adsorption of BSA to the surface of GNRs (AR 3.5) dispersed in nanopure deionized water by monitoring wavelength shifts in the λ_{max} over a time scale of 0−1000 s (Figure 3a).

The three functionalized GNRs (PAH, PAA, and PEG) showed very different BSA binding kinetics. We observed a "slow" adsorption process of BSA to PAA−GNRs and PEG−GNRs, with minimal change in the λ_{max} over the first 1000s of BSA−GNR interaction. However, the adsorption process is apparently faster on the surface of PAH-GNRs (with a λ_{max} shift of ∼20 nm observed in less than 10 s). Thus, it appears that BSA binding to the positively charged PAH-GNRs is much more rapid than the negatively charged (PAA) or neutral (PEG) GNRs, under the conditions studied here. Using a modified pseudo-second-order kinetic model,[35,36] which assumes that the BSA concentration is present in excess, the adsorption kinetic curve of the PAH−GNRs was successfully fitted to extract a rate constant (Figure 3b):

dx.doi.org/10.1021/la402920f | *Langmuir* XXXX, XXX, XXX−XXX

$$t/\Delta\lambda = t/\Delta\lambda_e + 1/k_2(\Delta\lambda_e)^2 \quad (1)$$

where k_2 is the second-order rate constant, t is time, and $\Delta\lambda$ and $\Delta\lambda_e$ are the shifts in plasmon wavelength at time t and after equilibrium is reached, respectively. Using this model, we found k_2 to be equal to $\sim 10^{-3}$ s^{-1} per nm plasmon shift for BSA adsorbing to PAH−GNRs. Unfortunately, the plasmon band shifts for both PAA−GNRs and PEG−GNRs were too small and slow to be amenable to the same analysis. Thus far, there have been very few studies that have determined a rate constant for BSA binding to GNRs; however, the observed time scales agree well with other rate constants that have previously been determined for protein association and exchange on functionalized NPs using surface plasmon resonance of nanoparticles bound to flat gold surfaces.[14]

This kinetic analysis indicates that BSA binds to and saturates the surface of PAH−GNRs much more rapidly than do PAA− or PEG−GNRs. For PAH−GNRs, BSA appears to saturate the GNR surface after only several minutes. For the PAA− and PEG−GNRs (under the same conditions), it appears that surface saturation by BSA requires a much longer time frame (1 h or more). At equilibrium, only PAH−GNRs show a significant red shift ($\Delta \approx 20$ nm) of their plasmon bands. PAA−GNRs only show a slight red shift ($\Delta \approx 5$ nm), whereas PEG−GNRs show no significant shift even at equilibrium. It should be noted that while the plasmon λ_{max} for the PAH−GNRs shows a large red shift following BSA adsorption, there is no evidence of peak broadening, nor a significant rise in the baseline of the spectrum, indicating that the change in the LSPR λ_{max} is primarily due to BSA binding, rather than GNR aggregation. These data suggest that electrostatics may strongly influence the amount of BSA that binds to the GNPs and/or the rate of the adsorption process. Having established a rough time scale for the binding of BSA to the GNP surface to reach saturation, we next set out to determine the equilibrium binding constants for BSA on the different GNP surfaces.

Fluorescence Quenching of BSA on GNPs: Global Change. The affinity of BSA for the functionalized GNP probes in this study was determined using two different analytical techniques: static fluorescence quenching and affinity capillary electrophoresis (ACE). These two analytical methods provide independent determinations of the equilibrium binding constant (K_a) between BSA and functionalized GNPs. While static fluorescence quenching relies on the optical properties of protein and GNPs, ACE determines the equilibrium binding constant on the basis of the charge-to-size ratio of the BSA−GNP complex. GNP−BSA binding constants were measured under equilibrium binding conditions, after BSA had sufficient time to saturate the GNP surfaces.

Given that metallic nanoparticles quench molecular fluorescence within 10 nm of their surface, fluorescence quenching experiments can be employed to quantify the adsorption process of fluorescent proteins to GNPs.[22] One major advantage is that the static fluorescence quenching method allows for the determination of binding constants without the need to separate free and bound proteins. It is assumed that the adsorption of proteins onto GNPs quenches the protein fluorescence.[17,37] However, care must be taken to specifically select proteins that have a significant fluorescent signal. In the case of BSA, which has two tryptophan residues, Trp-134 and Trp-212, the fluorescent signal is relatively strong.[38] By titrating GNPs into a BSA solution, the decrease in fluorescence intensity of BSA with respect to GNP concentration can be tabulated and quantified. In our experiments, BSA was fixed at 0.66 μM, and the GNP solution was added with the final GNP concentration being 0.02−3.0 nM. This translates to a BSA/GNP ratio ranging from 220 to 33 000. On the basis of simple geometric calculations, monolayer coverage of BSA on GNP surface can be approximated at 100 BSA molecules on 20 nm gold nanospheres, 220 BSA molecules on gold nanorods (AR 3.5), and 1800 BSA molecules on gold nanorods (AR 18). The initial fluorescence quenching titration experiments were performed in nanopure deionized water to minimize GNP aggregation following BSA binding, and to permit better comparisons with previous studies of BSA−GNP binding.

On the basis of the loss of fluorescence observed upon GNP titration into the BSA solution, we calculate that ∼1000−3000 BSA proteins bind to each gold nanorod (AR 3.5) depending on the initial BSA:GNP concentration ratio (Figure 4a,c,e). This indicates that BSA binding to GNPs continues beyond the formation of an initial monolayer, and that cooperative binding interactions between BSA molecules may be important interactions in the formation of the protein corona. It should be noted that under the conditions tested here, no GNPs aggregation was observed following BSA binding.

On the basis of a static quenching model, the fluorescence lifetime of the protein is assumed to be unaltered because GNP−protein complexes do not fluoresce. Therefore, we can use the Stern−Volmer relationship as follows:[17,39]

$$\frac{F_0}{F} = 1 + K_{SV}[\text{GNPs}] \quad (2)$$

where F_0 is the total fluorescence of BSA (in the absence of GNPs), F is the fluorescence of BSA at a specific nanoparticle concentration, and K_{sv} refers to the Stern−Volmer quenching constant. Figure 4a,c,e shows the fluorescence spectra of BSA incubated with increasing concentration of GNRs of aspect ratio 3.5 and different surface chemistries. The presence of GNPs causes the fluorescence of BSA to decrease. The concentration of the GNPs in the solution was increased to a saturation point, at which minimal fluorescence from BSA was detected. If we assume static quenching, where BSA and GNPs form a stable complex, K_{sv} becomes K_a (the association constant).[40] The Hill equation can be used to quantify the relationship between the fluorescence intensity and GNP concentration:

$$\log \frac{(F_0 - F)}{F - F_{sat}} = \log K_a + n \log[\text{GNP}] \quad (3)$$

where F_{sat} refers to the fluorescence of BSA at GNP saturation. The Hill coefficient, n, describes the degree of cooperativity in protein (ligand) binding to a surface.[41] If $n > 1$, the binding of a ligand is enhanced if there are already other ligands adsorbed to the surface. If $n < 1$, the binding of a ligand is decreased if there are already other ligands adsorbed to the surface. In cases where $n = 1$, the binding of a ligand is independent of other ligands already at the surface. By plotting a double logarithmic plot of $\log [(F_0 - F)/(F - F_{sat})]$ versus log[GNPs], K_a and n can be calculated from the y-intercept and gradient of the line of best fit (Figure 4). From those binding curves, we calculated binding constants (K_a) of $(1.48 \pm 0.25) \times 10^{10}$ M^{-1}, $(0.95 \pm 0.09) \times 10^{10}$ M^{-1}, and $(0.51 \pm 0.02) \times 10^{10}$ M^{-1} for PAH−GNRs, PAA−GNRs, and PEG−GNRs, respectively. Hill coefficients (cooperativity of binding) were also derived (n): 1.18 ± 0.12,

dx.doi.org/10.1021/la402920f | Langmuir XXXX, XXX, XXX−XXX

Table 1. Binding Constants (K_a) and Hill Coefficients (n) for GNPs of Different Surface Charges with BSA in Water[a]

	gold nanoparticles								
	nanospheres			nanorods AR 3.5			nanorods AR 18		
	PAA	PAH	PEG	PAA	PAH	PEG	PAA	PAH	PEG
K_a ($\times 10^{10}$ M^{-1})	0.30 ± 0.04	1.71 ± 0.33	0.28 ± 0.01	0.95 ± 0.09	1.48 ± 0.25	0.51 ± 0.02	1.22 ± 0.08	2.75 ± 0.49	0.82 ± 0.54
n	0.93 ± 0.31	0.57 ± 0.04	1.36 ± 0.09	1.28 ± 0.04	1.18 ± 0.12	1.34 ± 0.20	1.11 ± 0.03	0.72 ± 0.15	1.16 ± 0.36

[a]Gold nanospheres were 20 nm in diameter. Gold nanorods of aspect ratio (AR) 3.5 and 18 were used. Either poylacrylic acid (PAA, anionic), polyallylamine hydrochloride (PAH, cationic), or methoxy-polyethylene glycol (PEG, neutral) was coated onto GNPs.

Table 2. Calculated Binding Constants (K_a) of BSA to Short GNRs (Aspect Ratio 3.5) in Water versus Buffer for Different Surface Chemistries

	PAA–GNRs	PAH–GNRs	PEG–GNRs
K_a (M^{-1}) in water	(0.95 ± 0.09) × 10^{10}	(1.48 ± 0.25) × 10^{10}	(0.51 ± 0.02) × 10^{10}
K_a (M^{-1}) in MOPS	(0.97 ± 0.02) × 10^{10}	(2.40 ± 0.19) × 10^{10}	(1.39 ± 0.13) × 10^{10}

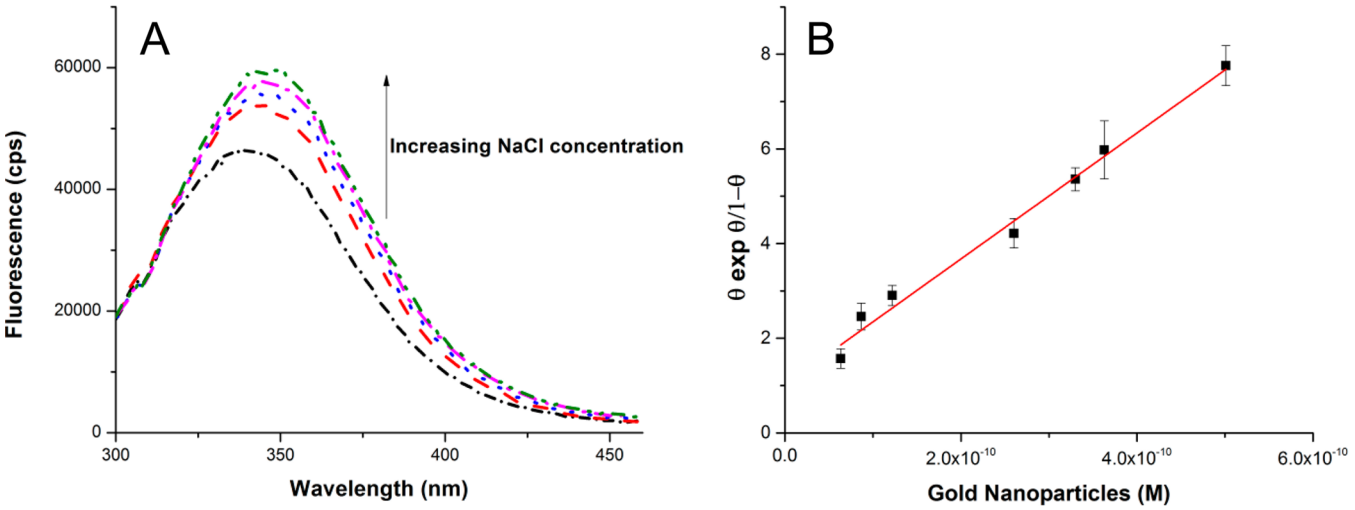

Figure 5. (A) Fluorescence spectra of BSA (0.5 μM) in the presence of PAH-coated gold nanospheres (20 nm) with varied NaCl concentration (0–5 mM). As the NaCl concentration increased, so does the fluorescence of BSA. (B) Frisch–Simha–Eirich plot for BSA adsorption to PAH-coated gold nanospheres to obtain K_{obs}. The best fit was obtained for K_1 = 0.5 and ν = 1.

1.28 ± 0.04, and 1.34 ± 0.20 for PAH–GNRs, PAA–GNRs, and PEG–GNRs. The experiment was repeated for longer GNR of aspect ratio ~18 and gold nanospheres of diameter around 20 nm (Supporting Information Figure S2). The equilibrium binding constants determined for all of these experiments are given in Table 1.

From the K_a values determined by the static fluorescence quenching method, three main trends were observed:

(1) The presence of PEG on the GNP surface did not prevent BSA adsorption over an extended incubation time. The affinities for all of the PEG-functionalized GNPs tested were similar to the binding constants determined for other GNPs regardless of shape.

(2) Regardless of GNP shape and size, PAH–GNPs had moderately higher affinities for BSA as compared to other GNP surfaces. It is likely that the overall negatively charged BSA (isoelectric point in water, pI 4.7)[28] is more strongly attracted to the positively charged PAH surface, suggesting that electrostatic interactions play a role in the binding process between BSA and the nanoparticle surface.

(3) Hill coefficients in most cases are higher than 1, suggesting cooperative binding. This is in agreement with the calculated number of BSA molecules bound to the GNPs, which is further evidence that BSA multilayers form on the GNPs.

Fluorescence Quenching of BSA on GNPs: Electrostatic Interactions. BSA contains 583 amino acids, with a net negative charge at pH 7. This suggests that the local electrostatic environment of ionizable amino acids, and hence BSA, can be altered by varying the ionic strength and pH of the medium.[42] As most BSA adsorption experiments are performed in various media without control or reporting of ionic strength, it is likely that some differences in the reported binding constants are due to the variations in BSA's ionizability. To investigate the contribution of ionic strength and pH, which both impact the electrostatic interactions of protein–nanoparticle binding, equilibrium binding constant determinations of BSA–GNPs were repeated in buffer (5 mM). As shown in Table 2, when fluorescence quenching titrations were repeated in buffer, the calculated K_a values were similar to values obtained in ultrapure water. This suggests that at pH 7 and 5 mM MOPS buffer, the ionic strength and pH contributions are not significant enough to alter the binding constants. We note that the Debye length in this buffer is 4 nm.

The contribution of the electrostatic interactions in the adsorption process was further probed by performing salt titration experiments.The sodium chloride was titrated into a

dx.doi.org/10.1021/la402920f | Langmuir XXXX, XXX, XXX–XXX

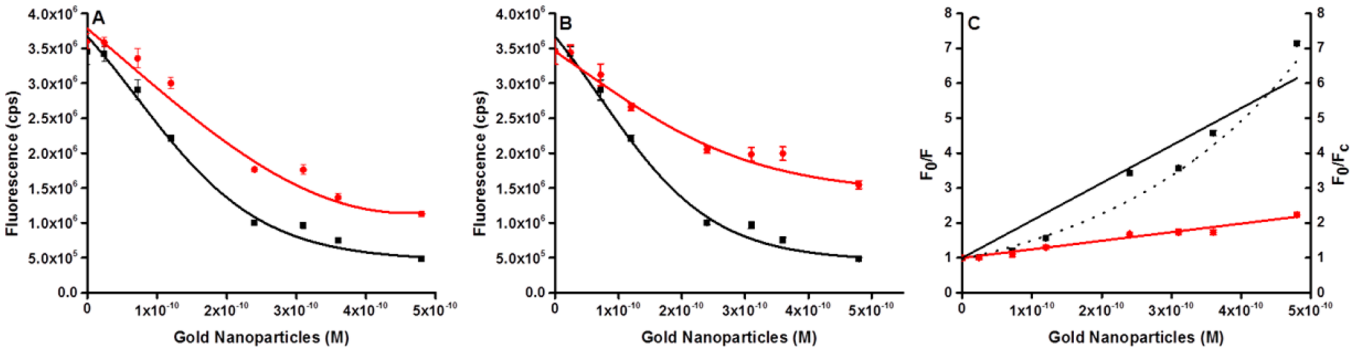

Figure 6. (A) Fluorescence quenching titrations of BSA in the presence of PAH gold nanorods (AR 3.5) (black) and with PAH gold nanorods presaturated with BSA (red). (B) Fluorescence quenching plots of BSA with PAH gold nanorods before (black) and after (red) correction. (C) Data points from fluorescence quenching titrations before (black) and after (red) correction was fitted using the Stern–Volmer relationship (solid lines). Uncorrected data points appear to fit a nonlinear curve better (dotted line). The left axis (F_0/F) corresponds to the uncorrected fluorescence data, while the right axis (F_0/F_C) corresponds to the IFE-corrected data.

gold nanoparticle–protein complex solution to alter the electrostatic interaction between PAH–GNPs (spheres) and BSA protein. Results showed that as the ionic strength of the solution was increased, a recovery of BSA fluorescence was observed (Figure 5A). We used the Frisch–Sihma–Eirich adsorption isotherm (FSE) to determine the electrostatic contribution to the binding of BSA to the surface of the GNPs, because it yielded the best fit for the salt titration experiments (as compared to the Langmuir adsorption isotherm and the Hill equation):[43] The basic form of the FSE adsorption isotherm is shown below:

$$\frac{\theta \exp(2K_1\theta)}{1-\theta} = (K_{obs}C)^{1/\nu} \quad (4)$$

where C is the concentration of GNPs; K_{obs} is the equilibrium constant for binding; K_1 and ν are parameters pertaining to the segment of polymer adsorbed because this model is based on adsorption of long polymers on flat surfaces; and θ represents the fractional change in luminescence and is equal to $[(F - F_0)/(F_{sat} - F_0)]$. Here, F is equal to the fluorescence at an arbitrary point. In our case, the values for C, K_{obs}, K_1, and ν were set to obtain the best possible fit. K_{obs} values at each salt concentration could be calculated by setting the parameters ν = 1 and K_1 = 0.5.[43,44] This model assumes that the decrease in fluorescence is proportional to surface coverage of the GNPs by BSA.[43]

Using polyelectrolyte theory,[45] the log of the K_{obs} values were plotted against the log of the salt concentrations to yield the slope *SK*. *SK* was used to calculate the electrostatic contribution to the free energy change upon binding (ΔG_{elec}) at each salt concentration using eq 5. ΔG_{obs} was calculated from the previous titration experiment performed for PAH–GNS, this time using the FSE adsorption isotherm to calculate K_{obs} for more accurate comparison, again setting the parameters ν = 1 and K_1 = 0.5 in eq 4. We used eq 6 to derive ΔG_{obs}. Figure 5B represents the binding isotherm obtained for PAH–GNS and BSA interaction using FSE.

$$\Delta G_{elec} = SK(RT)\ \ln[\mathrm{NaCl}] \quad (5)$$

$$\Delta G_{obs} = -RT\ \ln K_{obs} \quad (6)$$

In eqs 5 and 6, R is the gas constant and T is the temperature. Using the procedure above, the following values were obtained for the overall free energy of binding (ΔG_{obs}) and the electrostatic contribution to the free energy of binding (ΔG_{elec}), respectively: $\Delta G_{obs} = -56.9 \times 10^3$ J/mol and $\Delta G_{elec} = -11.5 \times 10^3$ J/mol. Therefore, the electrostatic contribution for the binding for BSA to the surface of PAH–GNPs is about 20% of the overall free energy of binding.

The increase of fluorescence from the BSA–GNP solution upon the addition of NaCl suggests that electrostatic interactions are a component of the many possible events that occur when BSA adsorbs onto GNPs (Figure 5). Interestingly, when the BSA–GNRs fluorescence quenching studies are performed in MOPS buffer, increased K_a values are observed for the PAH–GNRs and the PEG–GNRs, but not for the PAA–GNRs as compared to nanopure deionized water (Table 2). The change in the equilibrium binding constants determined in buffered solution highlights a potential complication in studying protein–GNP adsorption. The ionic strength of solution, within a certain range, can influence protein–GNP and protein–protein interactions. The presence of salts or buffer in solution could act to increase protein–protein interactions, decrease BSA–GNR interactions, or change the conformation of BSA in solution, opening new interaction sites for BSA–GNR binding. Therefore, the media in which fluorescence quenching studies are performed is an important point to consider in the design of protein–GNP binding investigations. While our results suggest that electrostatic interactions are only 20% of the overall equilibrium binding free energy, other forces such as London dispersion, hydrogen bonding, and release of bound water can also lead to protein adsorption.[46]

Fluorescence Quenching of BSA on GNPs: Inner Filter Effect from GNPs. While the large absorption coefficient and scattering of GNPs are favored in numerous applications, these effects complicate the use of GNPs in optical titration experiments. In the case of fluorescence quenching titrations, the high absorbance of GNPs can trivially absorb protein fluorescence even when the proteins are not closely bound to the surface. At even higher concentrations of GNPs, the presence of the GNP metal core can scatter the input and output fluorescence light, further reducing the fluorescence signal. These effects, which we term the inner filter effect (IFE), act together to produce a fluorescence quenching curve that is not representative of the actual binding of proteins to GNPs. We recently measured similar effects for surface-enhanced Raman scattering of molecules bound to gold nanorods in transmission mode.[47]

dx.doi.org/10.1021/la402920f | *Langmuir* XXXX, XXX, XXX–XXX

We have previously described a method to account for the IFE, such that the fluorescence quenching of proteins adsorbed on GNPs can be isolated.[26] In this method, fluorescence quenching of GNPs with proteins is performed twice, first using "clean" GNPs and again using GNP presaturated with protein. If the fluorescence quenching of presaturated GNP can be attributed to IFE, the difference in fluorescence quenching between these two plots can then be taken to isolate only proteins adsorbed in the hard corona of GNPs. Following this method, to probe the extent of influence from IFE, we can correct fluorescence quenching of BSA by PAH gold nanorods of aspect ratio 3.5 as an example.

Comparison of the fluorescence quenching titrations showed that when GNPs presaturated with BSA were used, greater fluorescence intensity was observed, which was more obvious at higher GNP concentrations (Figure 6). For comparison, both uncorrected and corrected titrations were fitted using the Stern–Volmer relationship and binding constants extracted. The K_a obtained for the uncorrected fluorescence quenching curve was $(1.07 \pm 0.08) \times 10^{10}$ M^{-1}, while after correction K_a was $(2.45 \pm 0.11) \times 10^{9}$ M^{-1}. Therefore, while the correction is not trivial,[48] it does not explain the 7 orders of magnitude difference in binding constant for BSA to gold nanoparticles across multiple laboratories by fluorescence (Table 3).

Table 3. Calculated Binding Parameters for Gold Nanorods with BSA, Using ACE in 5 mM MOPS

binding parameters	PAA–GNRs	PEG–GNRs
K_a (M^{-1})	$(7.93 \pm 0.49) \times 10^4$	$(1.53 \pm 0.09) \times 10^4$
n	2.29 ± 0.31	2.19 ± 0.27

Affinity Capillary Electrophoresis (ACE) To Probe GNP and BSA Interactions. The potential optical interference that GNPs produce in fluorescence-based binding assays (via the IFE) was a significant source of concern in our determination of the equilibrium binding constants. Accordingly, we explored a number of other methods to determine the protein–nanoparticle binding constants besides fluorescence. Isothermal titration calorimetry (ITC) and surface plasmon resonance (SPR) gave irreproducible results, mostly likely due to the low concentrations of gold nanoparticle solutions required to avoid particle aggregation. A nonoptical method, such as affinity capillary electrophoresis, then became of interest. Classical ACE[41,48] has been utilized to evaluate the interaction between GNPs and BSA as a comparative method to steady-state fluorescence measurements, although overall there have been very few measurements performed on nanoparticle–protein systems with this technique.[40,41]

There are several advantages to measuring the dissociation constant of the GNP–BSA complex by capillary electrophoresis. The capillary electrophoresis separations of NP–protein complexes are rapid, and consume low volumes of reagent and sample.[42] In addition, this approach does not rely on optical spectroscopy to determine the equilibrium dissociation constants associated with protein–NP interactions, but rather relies on the charge-to-size ratio of the protein–NP complex. The capillary electrophoresis approach is convenient to make comparisons across different NP sizes or different NP core materials, as it is unnecessary to correct for optical interferences.

In this work, capillary electrophoresis runs were completed in 7 min using 20 μL volumes of nanoparticle solution. For these experiments, we primarily studied the BSA binding behavior of the low aspect ratio gold nanorods (AR 3.5). In the absence of protein in the background electrolyte, the migration velocity of gold nanorods, defined as $v = \mu_a E$, is a function of the apparent mobility, μ_a, and the applied electric field, E. The apparent mobility is the sum of the bulk electroosmotic flow, μ_{eof}, which occurs as a consequence of the charged capillary surface and applied field, and of the analyte electrophoretic mobility, μ_{eph}, related to the ratio of the charge and hydrodynamic radius.[49] As the charge-to-size ratio of the protein–nanoparticle complex differs from that of the free nanoparticle, the migration velocity of complex differs from the free nanoparticle.[44] The migration time reflects the amount of time the nanoparticle is bound to protein.

The GNP–BSA dissociation constants for various types of nanoparticles were determined by changing the amount of protein ligand present during the separation and by measuring the fraction of the nanoparticle that exists as a complex. This fraction, f_1, which describes the ratio of the bound nanoparticle to total nanoparticle, is fit to a hyperbolic binding isotherm using nonlinear regression. The ratio f_1 was derived from the change in migration time associated with change in the concentration of the protein ligand in the background electrolyte. The equation used for rapidly equilibrating receptor and ligand has been previously reported as:[48,50]

$$\mu_{app} = f_1 \mu_{max} + f_2 \mu_{free} \quad (7)$$

where μ_{app} is the apparent mobility of the nanoparticle measured using a specific concentration of ligand in the background electrolyte, μ_{max} is the mobility of the nanoparticle–protein complex, μ_{free} is the mobility of free nanoparticles, and f_2 is the fraction that is free. The above equation is simplified by substituting the variable f_2 with $(1 - f_1)$ and then rearranged as $f_1 = (\mu_{app} - \mu_{free})/(\mu_{max} - \mu_{free})$. Dissociation constant, K_D, which relates the forward and reverse rate constants for the binding of acceptor (i.e.,

Table 4. Published Binding Constants of GNPs for BSA As Reported by Different Research Groups[a]

nanoparticle	shape	size (nm)	solvent	method	K_a (M^{-1})	author
citrate–GNP	sphere	18	water	fluorescence	2.34×10^{11}	Iosin et al. (2009)[37]
CTAB–GNP	rod	70 × 30	water	fluorescence	5.0×10^4	Iosin et al. (2009)[37]
Glut–GNP	sphere	40	PBS	fluorescence	3.16×10^{11}	Wangoo et al. (2008)[52]
citrate–GNP	sphere	20	water	CD	7.14×10^8	Truel et al. (2010)[53]
citrate–GNP	sphere	10	water	QCM	1.0×10^6	Brewer et al. (2005)[23]
citrate–GNP	sphere	15	PBS	fluorescence	3.0×10^9	Shang et al. (2007)[54]
citrate–GNP	sphere	51	HEPES	SCS	4.0×10^3	Dominguez-Medina et al. (2012)[55]

[a]PBS = phosphate buffered saline; CD = circular dichroism; QCM = quartz crystal microbalance; SCS = scattering correlation spectroscopy.

dx.doi.org/10.1021/la402920f | Langmuir XXXX, XXX, XXX–XXX

nanoparticle) and protein ligand, is derived using the Hill equation.

$$f_1 = [\text{protein}]^n/(K_D{}^n + [\text{protein}]^n) \quad (8)$$

Again here, the Hill coefficient (n) describes binding cooperativity. Equations 7 and 8 model the homogeneous binding interaction between ligand and acceptor in cases where complex formation occurs without an intermediate state or with a short-lived intermediate.[41,50]

The parameters described by eqs 7 and 8 were determined experimentally with ACE to derive the binding parameters for both PAA−GNRs and PEG−GNRs using a bare fused silica capillary. The electroosmotic flow decreased when the BSA was included in the background electrolyte due to nonspecific adsorption to the capillary surface. Therefore, the capillary surface was renewed between each separation, and the electroosmotic flow was measured for each separation run using a neutral marker, dimethylformamide, detected at 214 nm. The electrophoretic mobility of protein nanorod complex was determined by subtracting the electroosmotic flow from the apparent mobility (Supporting Information Figures S3 and S6). Results are summarized in Table 4. A shift in the mobility of the PAA−GNRs (7.4 nM), detected at 300 nm, was measured using background electrolyte (5 mM MOPS) containing BSA ranging from 0 to 50 μM (Figure 7). The

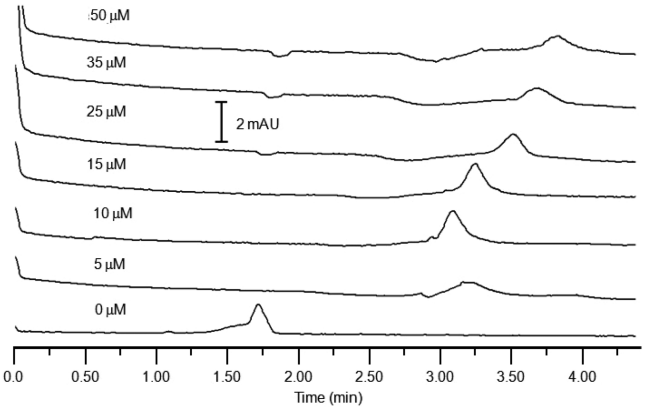

Figure 7. Electropherogram of PAA−GNRs (7.4 nM) detected at 300 nm with BSA, as listed, in 5 mM MOPS buffer. Concentrations of BSA in the background electrolyte increase from 0 μM (lower trace) to 50 μM (upper trace). At different concentrations of BSA in the running buffer (0, 5, 10, 15, 25, 35, 50 μM), a shift in the apparent mobility of the GNRs is observed.

data were fit to eq 8 (Figure 8) yielding binding constants (K_a) of (7.93 ± 0.49) × 10^4 and (1.53 ± 0.09) × 10^4 M^{-1} for PAA−GNRs and PEG−GNRs, respectively (Supporting Information Figures S4−S6). Hill coefficients were found to be 2.28 ± 0.31 and 2.19 ± 0.27 for PAA−GNRs and PEG−GNRs, respectively. This technique also confirms the adsorption of protein to the surface of pegylated GNPs with the same level of affinity as for other surface types. We were not able to calculate a binding constant for PAH−GNRs, possibly due to the strong interaction of the positively charged particles with the inner wall of the capillary. Furthermore, the strong interaction of PAH−GNRs with the BSA protein caused a rapid aggregation of the nanomaterials in the presence of BSA.

The binding constants obtained using ACE were significantly lower than the binding constants determined by our static

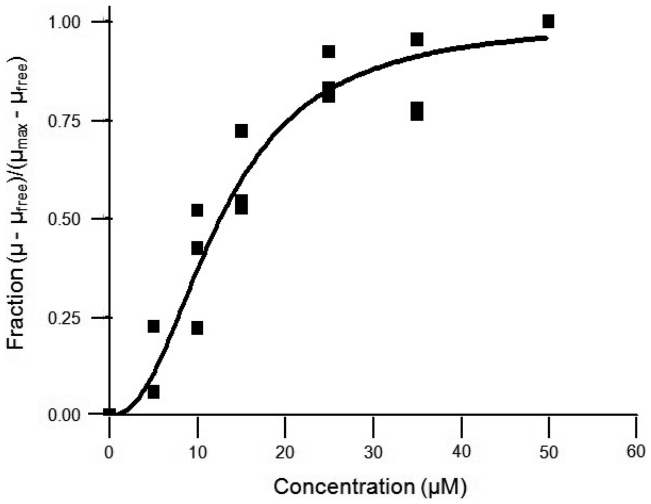

Figure 8. Titration curve for PAA−GNRs with BSA, as measured by ACE. The dissociation constant is derived from the curve fit using pooled data from PAA−GNRs (7.4 nM) detected at 300 nm with increasing concentration of BSA in 5 mM MOPS buffer. The pooled data are a combination of all points from three replicate curves.

fluorescence quenching experiments. Again, however, the K_a values were comparable between the PEG and PAA−GNRs. Similar to the fluorescence measurements, the calculated Hill coefficients are higher than 1, which suggests cooperative binding of BSA to nanoparticle surfaces. However, ACE yielded 10^5× lower binding affinities as compared to steady-tate fluorescence measurements in this work. The values calculated are within the range of what as been reported using other techniques; for example, Lacerda et al. reported binding constants ranging between 10^4−10^7 M^{-1} for plasma proteins adsorbing to gold nanospheres, based on measurements made using static fluorescence quenching.[51]

Determining the equilibrium binding constants of BSA adsorbed to GNPs by ACE has several advantages over the static fluorescence quenching technique. Similar to fluorescence quenching, ACE is capable of differentiating between BSA−GNR complexes and free GNRs without the need to separate free and bound protein, simply by looking at the shift in mobility. Unlike static fluorescence quenching, however, there is no issue with spectral interference due to the presence of GNRs. Instead, the primary challenge in using ACE to determine protein−GNP binding constants is a materials compatibility issue. In our experiments, positively charged GNPs adhered strongly to the inner surface of the capillary. This prevented an accurate determination of the binding constant for proteins bound to positively charged GNPs. Further study of this method with capillaries presenting a more inactive inner surface could limit GNPs interacting with the capillary and help improve the versatility of the technique. On the other hand, the steady-state fluorescence approach presented in the first part of this Article is quite versatile in the different types of gold nanoparticles that can be analyzed; however, it relies on the fluorescence capabilities of the protein and suffers from significant GNPs optical interference. Last, only NPs that strongly quench single molecule fluorescence (such as GNPs) can be studied by the fluorescence quenching method.

An analysis of the literature shows that there is a significant discrepancy in reported gold nanoparticle−protein binding constants, which fall anywhere from 10^4 to 10^{11} M^{-1}.[24,37,52] Our

dx.doi.org/10.1021/la402920f | Langmuir XXXX, XXX, XXX−XXX

results are within this range when compared to other publications using the fluorescence quenching approach. Typically, nonfluorescence-based methods such as circular dichroism spectroscopy and quartz crystal microbalance have yielded lower binding constant values than fluorescence-based techniques (Table 4). We observed a similar result, with the binding constants we determined by ACE being significantly lower than the binding constants determined by static fluorescence quenching for the same system, even for the same buffer. This may be due to the nature of the experiment: ACE is done in flow, and BSA is competing for binding sites on both the GNPs and the capillary walls. Thus, the difference in equilibrium between protein−wall and protein−GNP is really what is being measured.

A larger message is that the equilibrium binding constants that we determined both by static fluorescence quenching and by affinity capillary electrophoresis indicate that BSA binds with comparable affinity (same order of magnitude) to PEG-functionalized GNPs as compared to charged GNPs. This initially seems to be a surprising result, because PEG is considered to be an excellent antifouling agent, and PEG-functionalized surfaces are considered to be almost "protein proof".[56−58] Recently, new reports have emerged that indicate that the presence of PEG on GNP surfaces is not sufficient to eliminate protein adsorption, and that measurable protein adsorption can be detected within 24 h of PEG−GNP incubation in serum.[59]

Another recent paper reports that the aggregation-prone A-beta peptide binds surprisingly well to PEGylated polymer nanoparticles, with association constants of 6.2×10^3 M^{-1} from surface plasmon resonance measurements and 1.8×10^6 M^{-1} from capillary electrophoresis coupled with laser-induced detection (CE-LIF) measurements, for the peptide monomer.[60] In this case, the CE-LIF measurements were only able to monitor the loss of free peptide monomer as polymer nanoparticles were added, not free and bound nanoparticles, and peptide aggregation, of course, affected free peptide monomer concentrations. The authors of that paper attribute the orders-of-magnitude difference in binding constants to intrinsic differences in the techniques (e.g., flow rates, adsorption buildup, etc.).

CONCLUSION

In this work, two different techniques (fluorescence spectroscopy and affinity capillary electrophoresis) were used to derive binding constants and Hill coefficients for the adsorption of BSA onto the surface of functionalized gold nanospheres and nanorods. Within each technique, similar binding constants, within an order of magnitude, were observed no matter what the nanoparticle shape or surface charge, even for neutral PEG. Thus, we might say that BSA (known to stick to everything) beats PEG (supposed to resist protein adsorption).

While either technique (fluorescence or ACE) is theoretically suited to measure the BSA-GNP equilibrium binding constants, the K_a for BSA adsorption determined by each technique differed by orders of magnitude. Steady-state fluorescence measurements suffer from inner filter effects. Therefore, there is a need to develop efficient optical filtering setups or software to accurately pull out the binding parameters during the adsorption process of proteins. ACE, in our opinion, ought to be one of the most reliable methods to investigate the adsorption of protein to the surface of gold nanoparticles because the mobility of the GNPs is probed directly using absorbance measurements, without preseparation steps, and it does not suffer from GNP optical interference. However, the analysis of positively charged gold nanoparticles by ACE remains a challenge due to inner capillary wall effects. We envisage that further experimentation with this technique using capillaries with different inner surface chemistries will allow the development of better methods with the goal of calculating binding parameters for a wide range of proteins to a wide range of nanoparticles.

ASSOCIATED CONTENT

Supporting Information

UV−vis absorbance measurements of gold nanospheres and GNRs AR 18. Double logarithmic plot for gold nanospheres and GNRs AR 18. ACE data for PEG−GNRs. This material is available free of charge via the Internet at http://pubs.acs.org.

AUTHOR INFORMATION

Corresponding Author

*Tel.: (217) 333-7680. E-mail: murphycj@illinois.edu.

Notes

The authors declare no competing financial interest.

ACKNOWLEDGMENTS

We thank Dr. Kenneth Suslick for access to the fluorescence spectrophotometer and Dr. Yi Lu for access to the diode array UV−visible absorbance spectrophotometer. Funding from the National Science Foundation (CHE-1011980, CHE-1306596) is gratefully acknowledged. We also acknowledge support for T.A.D. from the National Science Foundation (Cooperative Agreement 1003907).

REFERENCES

(1) Jain, P. K.; Huang, X.; El-Sayed, I. H.; El-Sayed, M. A. Noble Metals on the Nanoscale: Optical and Photothermal Properties and Some Applications in Imaging, Sensing, Biology, and Medicine. *Acc. Chem. Res.* **2008**, *41*, 1578−1586.

(2) Murphy, C. J.; Sau, T. K.; Gole, A. M.; Orendorff, C. J.; Gao, J.; Gou, L.; Hunyadi, S. E.; Li, T. Anisotropic Metal Nanoparticles: Synthesis, Assembly, and Optical Applications. *J. Phys. Chem. B* **2005**, *109*, 13857−13870.

(3) Murphy, C. J.; Gole, A. M.; Stone, J. W.; Sisco, P. N.; Alkilany, A. M.; Goldsmith, E. C.; Baxter, S. C. Gold Nanoparticles in Biology: Beyond Toxicity to Cellular Imaging. *Acc. Chem. Res.* **2008**, *41*, 1721−1730.

(4) Daniel, M.; Astruc, D. Gold Nanoparticles: Assembly, Supramolecular Chemistry, Quantum-Size-Related Properties, and Applications Toward Biology, Catalysis, and Nanotechnology. *Chem. Rev.* **2004**, *104*, 293−346.

(5) Lal, S.; Clare, S. E.; Halas, N. J. Nanoshell-Enabled Photothermal Cancer Therapy: Impending Clinical Impact. *Acc. Chem. Res.* **2008**, *41*, 1842−1851.

(6) Lynch, I.; Dawson, K. A. Protein-Nanoparticle Interactions. *Nano Today* **2008**, *3*, 40−47.

(7) Lynch, I.; Cedervall, T.; Lundqvist, M.; Cabaleiro-Lago, C.; Linse, S.; Dawson, K. A. The Nanoparticle - Protein Complex as a Biological Entity; a Complex Fluids and Surface Science Challenge for the 21st Century. *Adv. Colloid Interface Sci.* **2007**, *134*−*35*, 167−174.

(8) Ghosh, P.; Han, G.; De, M.; Kim, C. K.; Rotello, V. M. Gold Nanoparticles in Delivery Applications. *Adv. Drug Delivery Rev.* **2008**, *60*, 1307−1315.

(9) Nel, A. E.; Maedler, L.; Velegol, D.; Xia, T.; Hoek, E. M. V.; Somasundaran, P.; Klaessig, F.; Castranova, V.; Thompson, M. Understanding Biophysicochemical Interactions at the Nano-Bio Interface. *Nat. Mater.* **2009**, *8*, 543−557.

(10) Lesniak, A.; Fenaroli, F.; Monopoli, M. P.; Åberg, C.; Dawson, K. A.; Salvati, A. Effects of the Presence or Absence of a Protein Corona on Silica Nanoparticle Uptake and Impact on Cells. *ACS Nano* **2012**, *6*, 5845−5857.
(11) Lartigue, L.; Wilhelm, C.; Servais, J.; Factor, C.; Dencausse, A.; Bacri, J.-C.; Luciani, N.; Gazeau, F. Nanomagnetic Sensing of Blood Plasma Protein Interactions with Iron Oxide Nanoparticles: Impact on Macrophage Uptake. *ACS Nano* **2012**, *6*, 2665−2678.
(12) de Jong, W. H.; Hagens, W. I.; Krystek, P.; Burger, M. C.; Sips, A. J. A. M.; Geertsma, R. E. Particle Size-Dependent Organ Distribution of Gold Nanoparticles After Intravenous Administration. *Biomaterials* **2008**, *29*, 1912−1919.
(13) Johnston, H. J.; Hutchison, G.; Christensen, F. M.; Peters, S.; Hankin, S.; Stone, V. A Review of the in Vivo and in Vitro Toxicity of Silver and Gold Particulates: Particle Attributes and Biological Mechanisms Responsible for the Observed Toxicity. *Crit. Rev. Toxicol.* **2010**, *40*, 328−346.
(14) Cedervall, T.; Lynch, I.; Lindman, S.; Berggard, T.; Thulin, E.; Nilsson, H.; Dawson, K. A.; Linse, S. Understanding the Nanoparticle-Protein Corona Using Methods to Quantify Exchange Rates and Affinities of Proteins for Nanoparticles. *Proc. Natl. Acad. Sci. U.S.A.* **2007**, *104*, 2050−2055.
(15) Aubin-Tam, M. E.; Hamad-Schifferli, K. Gold Nanoparticle−Cytochrome C Complexes: the Effect of Nanoparticle Ligand Charge on Protein Structure. *Langmuir* **2005**, *21*, 12080−12084.
(16) Deka, J.; Paul, A.; Chattopadhyay, A. Estimating Conformation Content of a Protein Using Citrate-Stabilized Au Nanoparticles. *Nanoscale* **2010**, *2*, 1405−1412.
(17) Jhonsi, M. A.; Kathiravan, A.; Renganathan, R. Spectroscopic Studies on the Interaction of Colloidal Capped CdS Nanoparticles with Bovine Serum Albumin. *Colloids Surf., B* **2009**, *72*, 167−172.
(18) Iosin, M.; Canpean, V.; Astilean, S. Spectroscopic Studies on pH- and Thermally Induced Conformational Changes of Bovine Serum Albumin Adsorbed Onto Gold Nanoparticles. *J. Photochem. Photobiol., A* **2011**, *217*, 395−401.
(19) Pramanik, S.; Banerjee, P.; Sarkar, A.; Bhattacharya, S. C. Size-Dependent Interaction of Gold Nanoparticles with Transport Protein: a Spectroscopic Study. *J. Lumin.* **2008**, *128*, 1969−1974.
(20) Tsai, D. H.; Delrio, F. W.; Keene, A. M.; Tyner, K. M.; Maccuspie, R. I.; Cho, T. J.; Zachariah, M. R.; Hackley, V. A. Adsorption and Conformation of Serum Albumin Protein on Gold Nanoparticles Investigated Using Dimensional Measurements and in Situ Spectroscopic Methods. *Langmuir* **2011**, *27*, 2464−2477.
(21) Lundqvist, M.; Nygren, P.; Jonsson, B.-H.; Broo, K. Induction of Structure and Function in a Designed Peptide Upon Adsorption on a Silica Nanoparticle. *Angew. Chem., Int. Ed.* **2006**, *45*, 8169−8173.
(22) Sen, T.; Haldar, K. K.; Patra, A. Au Nanoparticle-Based Surface Energy Transfer Probe for Conformational Changes of BSA Protein. *J. Phys. Chem. C* **2008**, *112*, 17945−17951.
(23) Brewer, S.; Glomm, W.; Johnson, M.; Knag, M.; Franzen, S. Probing BSA Binding to Citrate-Coated Gold Nanoparticles and Surfaces. *Langmuir* **2005**, *21*, 9303−9307.
(24) Gomes, I.; Santos, N. C.; Oliveira, L. M. A.; Quintas, A.; Eaton, P.; Pereira, E.; Franco, R. Probing Surface Properties of Cytochrome C at Au Bionanoconjugates. *J. Phys. Chem. C* **2008**, *112*, 16340−16347.
(25) Orendorff, C. J.; Murphy, C. J. Quantitation of Metal Content in the Silver-Assisted Growth of Gold Nanorods. *J. Phys. Chem. B* **2006**, *110*, 3990−3994.
(26) Yang, J. A.; Johnson, B. J.; Wu, S.; Woods, W. S.; George, J. M.; Murphy, C. J. Study of Wild-Type A-Synuclein Binding and Orientation on Gold Nanoparticles. *Langmuir* **2013**, *29*, 4603−4615.
(27) Alkilany, A. M.; Lohse, S. E.; Murphy, C. J. The Gold Standard: Gold Nanoparticle Libraries to Understand the Nano−Bio Interface. *Acc. Chem. Res.* **2012**, *46*, 650−661.
(28) Peters, T., Jr. The Albumin Molecule. *Sciencedirect.com*; Elsevier: New York, 1995; pp 9-II.
(29) Jana, N.; Gearheart, L.; Murphy, C. Seed-Mediated Growth Approach for Shape-Controlled Synthesis of Spheroidal and Rod-Like Gold Nanoparticles Using a Surfactant Template. *Adv. Mater.* **2001**, *13*, 1389−1393.
(30) Sau, T. K.; Murphy, C. J. Seeded High Yield Synthesis of Short Au Nanorods in Aqueous Solution. *Langmuir* **2004**, *20*, 6414−6420.
(31) Jana, N. R.; Gearheart, L.; Murphy, C. J. Wet Chemical Synthesis of High Aspect Ratio Cylindrical Gold Nanorods. *J. Phys. Chem. B* **2001**, *105*, 4065−4067.
(32) Jana, N. R.; Gearheart, L.; Murphy, C. J. Seeding Growth for Size Control of 5−40 Nm Diameter Gold Nanoparticles. *Langmuir* **2001**, *17*, 6782−6786.
(33) Gole, A.; Murphy, C. J. Polyelectrolyte-Coated Gold Nanorods: Synthesis, Characterization and Immobilization. *Chem. Mater.* **2005**, *17*, 1325−1330.
(34) Fernández-López, C.; Mateo-Mateo, C.; Álvarez-Puebla, R. A.; Pérez-Juste, J.; Pastoriza-Santos, I.; Liz-Marzán, L. M. Highly Controlled Silica Coating of PEG-Capped Metal Nanoparticles and Preparation of SERS-Encoded Particles. *Langmuir* **2009**, *25*, 13894−13899.
(35) Ho, Y. S.; McKay, G. Pseudo-Second Order Model for Sorption Processes. *Process Biochem.* **1999**, *34*, 451−465.
(36) Khan, S. S.; Srivatsan, P.; Vaishnavi, N.; Mukherjee, A.; Chandrasekaran, N. Interaction of Silver Nanoparticles (SNPs) with Bacterial Extracellular Proteins (ECPs) and Its Adsorption Isotherms and Kinetics. *J. Hazard. Mater.* **2011**, *192*, 299−306.
(37) Iosin, M.; Toderas, F.; Baldeck, P. L.; Astilean, S. Study of Protein-Gold Nanoparticle Conjugates by Fluorescence and Surface-Enhanced Raman Scattering. *J. Mol. Struct.* **2009**, *924−26*, 196−200.
(38) Geddes, C. D. *Reviews in Fluorescence*; Springer: New York, 2009.
(39) Wang, C.; Wu, Q. H.; Li, C. R.; Wang, Z.; Ma, J. J.; Zang, X. H.; Qin, N.-X. Interaction of Tetrandrine with Human Serum Albumin: a Fluorescence Quenching Study. *Anal. Sci.* **2007**, *23*, 429−433.
(40) Lakowicz, J. R. *Principles of Fluorescence Spectroscopy*; Springer: New York, 2006.
(41) Weiss, J. N. The Hill Equation Revisited: Uses and Misuses. *FASEB J.* **1997**, *11*, 835−841.
(42) Wen, Y. P.; Dubin, P. L. Potentiometric Studies of the Interaction of Bovine Serum Albumin and Poly(Dimethyldiallylammonium Chloride). *Macromolecules* **1997**, *30*, 7856−7861.
(43) Mahtab, R.; Rogers, J. P.; Singleton, C. P.; Murphy, C. J. Preferential Adsorption of a "Kinked" DNA to a Neutral Curved Surface: Comparisons to and Implications for Nonspecific DNA−Protein Interactions. *J. Am. Chem. Soc.* **1996**, *118*, 7028−7032.
(44) Mahtab, R.; Rogers, J. P.; Murphy, C. J. Protein-Sized Quantum Dot Luminescence Can Distinguish Between "Straight", "Bent", and "Kinked" Oligonucleotides. *J. Am. Chem. Soc.* **1995**, *117*, 9099−9100.
(45) Mahtab, R.; Harden, H. H.; Murphy, C. J. Temperature-and Salt-Dependent Binding of Long DNA to Protein-Sized Quantum Dots: Thermodynamics of "Inorganic Protein-"DNA Interactions. *J. Am. Chem. Soc.* **2000**, *122*, 14−17.
(46) Xia, X. R.; Monteiro-Riviere, N. A.; Riviere, J. E. An Index for Characterization of Nanomaterials in Biological Systems. *Nat. Nanotechnol.* **2010**, *5*, 671−675.
(47) Sivapalan, S. T.; DeVetter, B. M.; Yang, T. K.; van Dijk, T.; Schulmerich, M. V.; Carney, P. S.; Bhargava, R.; Murphy, C. J. Off-Resonance Surface-Enhanced Raman Spectroscopy From Gold Nanorod Suspensions as a Function of Aspect Ratio: Not What We Thought. *ACS Nano* **2013**, *7*, 2099−2105.
(48) Li, N.; Zeng, S.; He, L.; Zhong, W. Probing Nanoparticle−Protein Interaction by Capillary Electrophoresis. *Anal. Chem.* **2010**, *82*, 7460−7466.
(49) Jorgenson, J. W.; Lukacs, K. D. Zone Electrophoresis in Open-Tubular Glass Capillaries. *Anal. Chem.* **1981**, *53*, 1298−1302.
(50) Colton, I. J.; Carbeck, J. D.; Rao, J.; Whitesides, G. M. Affinity Capillary Electrophoresis: a Physical-Organic Tool for Studying Interactions in Biomolecular Recognition. *Adv. Funct. Mater.* **1998**, *19*, 367−382.

(51) Lacerda, S. H. D. P.; Park, J. J.; Meuse, C.; Pristinski, D.; Becker, M. L.; Karim, A.; Douglas, J. F. Interaction of Gold Nanoparticles with Common Human Blood Proteins. *ACS Nano* **2010**, *4*, 365−379.
(52) Wangoo, N.; Suri, C. R.; Shekhawat, G. Interaction of Gold Nanoparticles with Protein: a Spectroscopic Study to Monitor Protein Conformational Changes. *Appl. Phys. Lett.* **2008**, *92*, 133104.
(53) Treuel, L.; Malissek, M.; Gebauer, J. S.; Zellner, R. The Influence of Surface Composition of Nanoparticles on Their Interactions with Serum Albumin. *ChemPhysChem* **2010**, *11*, 3093−3099.
(54) Shang, L.; Wang, Y.; Jiang, J.; Dong, S. pH-Dependent Protein Conformational Changes in Albumin:Gold Nanoparticle Bioconjugates: a Spectroscopic Study. *Langmuir* **2007**, *23*, 2714−2721.
(55) Dominguez-Medina, S.; McDonough, S.; Swanglap, P.; Landes, C. F.; Link, S. In Situ Measurement of Bovine Serum Albumin Interaction with Gold Nanospheres. *Langmuir* **2012**, *28*, 9131−9139.
(56) Otsuka, H.; Akiyama, Y.; Nagasaki, Y.; Kataoka, K. Quantitative and Reversible Lectin-Induced Association of Gold Nanoparticles Modified with A-Lactosyl-Ω-Mercapto-Poly(Ethylene Glycol). *J. Am. Chem. Soc.* **2001**, *123*, 8226−8230.
(57) Blümmel, J.; Perschmann, N.; Aydin, D.; Drinjakovic, J.; Surrey, T.; Lopez-Garcia, M.; Kessler, H.; Spatz, J. P. Protein Repellent Properties of Covalently Attached PEG Coatings on Nanostructured SiO2-Based Interfaces. *Biomaterials* **2007**, *28*, 4739−4747.
(58) Yeh, P-Y.J.; Kainthan, R. K.; Zou, Y.; Chiao, M.; Kizhakkedathu, J. N. Self-Assembled Monothiol-Terminated Hyperbranched Polyglycerols on a Gold Surface: a Comparative Study on the Structure, Morphology, and Protein Adsorption Characteristics with Linear Poly(Ethylene Glycol)s. *Langmuir* **2008**, *24*, 4907−4916.
(59) Larson, T. A.; Joshi, P. P.; Sokolov, K. Preventing Protein Adsorption and Macrophage Uptake of Gold Nanoparticles via a Hydrophobic Shield. *ACS Nano* **2012**, *6*, 9182−9190.
(60) Brambilla, D.; Verpillot, R.; Le Droumaguet, B.; Nicolas, J.; Taverna, M.; Kóna, J.; Lettiero, B.; Hashemi, S. H.; De Kimpe, L.; Canovi, M. PEGylated Nanoparticles Bind to and Alter Amyloid-Beta Peptide Conformation: Toward Engineering of Functional Nanomedicines for Alzheimer's Disease. *ACS Nano* **2012**, *6*, 5897−5908.